Computers, Materials & Continua CMC, vol.62, no.2, pp.679-694, 2020

A Deep Convolutional Architectural Framework for Radiograph Image Processing at Bit Plane Level for Gender & Age Assessment

N. Shobha Rani[1, *], M. Chandrajith[2], B. R. Pushpa[1] and B. J. Bipin Nair[1]

Abstract: Assessing the age of an individual via bones serves as a fool proof method in true determination of individual skills. Several attempts are reported in the past for assessment of chronological age of an individual based on variety of discriminative features found in wrist radiograph images. The permutation and combination of these features realized satisfactory accuracies for a set of limited groups. In this paper, assessment of gender for individuals of chronological age between 1-17 years is performed using left hand wrist radiograph images. A fully automated approach is proposed for removal of noise persisted due to non-uniform illumination during the process of radiograph acquisition process. Subsequent to this a computational technique for extraction of wrist region is proposed using operations on specific bit planes of image. A framework called GeNet of deep convolutional neural network is applied for classification of extracted wrist regions into male and female. The experimentations are conducted on the datasets of Radiological Society of North America (RSNA) of about 12442 images. Efficiency of preprocessing and segmentation techniques resulted into a correlation of about 99.09%. Performance of GeNet is evaluated on the extracted wrist regions resulting into an accuracy of 82.18%.

Keywords: Bit plane processing, automated segmentation, deep convolutional network.

1 Introduction

Age is a reflection of the level of development of bones, in this regard the bones present in left hand wrist region plays a dominant role due to its non-dominant usage in most of individual life.

Assessment of gender based on the bone development in wrist images is one of the challenging problems in pattern recognition. The several factors of bone development are employed in prediction of an individual ultimate height, gender, approximation of pubertal age of a child and in diagnosis of various growths related disorders [Pietka, Gertych, Pospiech et al. (2001)]. Assessing the gender of an individual via bones helps in archaeological and various crime investigations of forensic identification process [Santosh (2019)].

[1] Department of Computer Science, Amrita School of Arts and Sciences, Mysuru, Amrita Vishwa Vidyapeetham, India.

[2] Maharaja Institute of Technology, Mysuru, India.

[*] Corresponding Author: N. Shobha Rani. Email: n_shobharani@asas.mysore.amrita.edu.

Currently machine learning and artificial intelligence are the dominant technologies in providing automated solutions for various diagnosis related challenges. Identification of gender is based on exploration of relationships distal radius, ulna and lunate [Mwaturura, Cloutier and Daneshvar (2019)] and stated that aforesaid bones exhibit variability required for assessment. Expert knowledge from the Tanner and white house (TW3) technique and features of wrist radiographs are used for classification of bone age using Faster Convolutional Neural Networks (FCNN's) [Bui, Lee and Shin (2019)]. A morphometric analysis is conducted on the features of corpus callosum region of brain MRI images [Kontos, Megalooikonomou and Gee (2009)] for identification of gender using various statistical tests. Facial features and expressions also indicative of factors for differentiation of gender [Afifi and Abdelhamed (2019); Rai and Khanna (2014)]. It is obvious with the current developments that machine learning and artificial intelligence plays a vital role in automation of various real time problems.

In this work, the focus is mainly on classification of gender based on radiograph wrist images using deep learning architecture. Bae et al. [Bae and Jung (2018)] proposed a deep neural network architecture for bone age prediction using triplet loss function. Initially a hand segmentation network is built and a triplet sample is generated from each sample consisting of a target and evaluated performance RSNA bone age dataset which has reduced the error rate from 5.74 to 4.69% and from 5.89 to 4.85% in case of male and female age assessment. Though Triplet loss function model has shown some improvements in terms of accuracy, however, the evaluation on noisy samples are not addressed. A deep learning architecture is proposed [Wang, Shen, Shi et al. (2018)] based on the distal radius and ulna areas extracted separately from radiograph images and estimated the bone age. A comprehensive evaluation is conducted on both regions extracted individually resulting in 92% and 90% classification accuracies.

Bone Xpert system [Martin, Deusch, Schweizer et al. (2008)] developed based on shape-driven features of radius, ulna, and small bones. An appearance model of the about 3,000 bones are created using Gabor filters for children of age less than 1 year in 1989. Later HANDX system [Michael and Nelson (1989)] is developed to segment bones in wrist X-ray images using edge detection techniques. The bone lengths and other statistical features are employed as features for assessment of bone age. Based on the bone growth rate [Pietka, Gertych, Pospiech et al. (2001)] suggested a method to isolate Epiphyseal/Metaphyseal region for comparing it with chronological age to detect the skeletal maturity by using Atlas mapping and TW2. For accurately predicting the bone age, [Mahmoodi, Sharif, Chester et al. (2000)], in his work had devised a regression model and Bayesian estimator based on active shape models for bone age assessment of children belonging to age 1-16 year.

In a different work, Fuzzy ID3 decision tree is used by Aja et al. [Aja, Luis, Martın et al. (2004)] to classify radiographs into different age groups. The classifier is trained by set of primitive points and lines. Giordano et al. [Giordano, Leonardi, Maior et al. (2007)] proposed an EMROI feature extraction using DoG filter. Using TW3 method, a classification model for bone maturity state has been developed by Tristan et al. [Tristan and Arribas (2008)] by extracting 89 features from radius and ulna bones. These features are used for segmentation, feature extraction, neural networks for assessment of bone age. An analysis is conducted on carpal bones as well as epiphyseal and metaphyseal bones by

Giordano et al. [Giordano, Spampinato, Scarciofalo et al. (2010)] to predict the bone maturity sate of 0-10 years for males and 0-7 years for females. Fuzzy theory with principle component analysis is applied on carpal bones to estimate the maturity of skeletons.

Hsieh et al. [Hsieh, Liu, Jong et al. (2010); Villar, Alemán, Castillo et al. (2017)] proposed fuzzy-based growth model for bone age prediction and for age estimation from the pubic bone. Bag of features method along with random forest classifier is used for classification of features on phalanges bones by Simu et al. [Simu and Lal (2017)]. In a different work, Lee et al. [Lee, Tajmir, Lee et al. (2017)] proposed a method to extract the region of interest using deep learned pre-trained Image Net CNN. Also, a study on carpal and phalangeal bone analysis by Gertych et al. [Gertych, Zhang, Sayre et al. (2007)] proved that for boys of age 1-7 and girls from 1-5, carpel bone found to be efficient for bone age assessment and Phalangeal regions can be used for both male and female above age 13. Bull et al. [Bull, Edwards, Kemp et al. (1999)] carried out a comparative study on bone age assessment based on Greulich and Pyle, TW2 methods. 362 radiograph images are employed for study using TW2 method and found to be more accurate than Greulich and Pyle method.

Thangam et al. [Thangam, Mahendiran and Thanushkodi (2012)] described various alternative ways of developing a model for bone age assessment including fuzzy sets, dynamic thresholding, region based technique, bone labeling, Bayesian and regression Technique etc. Mansourvar et al. [Mansourvar, Ismail, Herawan et al. (2013)] surveyed on various challenges involved in bone age assessment related to birth documents and legal issues. Pietka et al. [Pietka, Kaabi, Kuo et al. (1993)] proposed a method for bone age assessment based on carpal bone features using thresholding techniques. Tanner et al. [Tanner and Gibbons (1994)] proposed a method using the physical changes and their rate of change as a measure to estimate the rate of maturation of bones.

As it is analyzed above, some of the critical observations from the literature in the proposed area of study are; i) poor efficiency of segmentation due to lack of image pre-processing protocols ii) Region of interest extraction is not fully automated that poses the main challenge for image segmentation, iii) Lack of preprocessing being noticed include hand-to-background ratio, hand orientation correction, limited success due to faint bone edges and iv) enhanced feature engineering to identify an optimal set of bones is lacking.

Few challenges in the non-technical point of view; i) Poor visibility of carpal bones in radiographs of very young children, ii) Lack of an established sequence of appearance of some of the carpal bones as the child grows iii) Discriminating the different levels of merges between these groups of ages iv) Overlap of phalangeal bones introduces challenges in the development of computer vision algorithms. As the perspective of gender classification may provide a reliable source for classification of gender for generically for the age groups of range 1-17.

In the reminder of the paper, Section 2 presents proposed methodology, section depicts the results of experimental analysis and finally Section 5 concludes the work.

2 Proposed methodology

In this work, as a part of initial pre-processing procedure a radiograph image I is subject to histogram equalization protocol $H(I)$ leading to even illumination effect on I. Let r indicate the intensity in a non-illumination image I and s denote the transformed gray level of uniformly illuminated image $\bar{I}$ obtained after implication of $H(I)$as given Eq. (1).

$$\bar{I} = H(I) \tag{1}$$

Specifically transformation with respect to a gray level is given by (2).

$$\bar{I}(s) = H(I(r)) \tag{2}$$

where s is subject to integral function of probability density of gray level in an image as given in (3)

$$s = \int_{0}^{r} \mathrm{P_r}(r)dr \tag{3}$$

Such that $L_{\min(I)} \le r \le L_{\max(I)}$ where $L_{\min(I)}$ and $L_{\max(I)}$ indicate the minimum and maximum gray levels in I and $L_{\min(\bar{I})} \le s \le L_{\max(\bar{I})}$ indicate $L_{\max(I)}$ indicate the minimum and maximum gray levels in $\bar{I}$ and $\mathrm{P_r}(r)dr$ is a cumulative density function that transforms the non-uniform illumination to flat or uniform illumination.

Further the equalized image $\bar{I}$ is directed for grainy noise removal using Gaussian filtering with a kernel of dimension 3×3. The effect of Gaussian smoothing lead to the suppression of grainy noise patterns in the image $\bar{I}$. Gaussian smoothing is an isotropic symmetric filter given by (4)

$$g(x,y) = \frac{1}{2\pi\sigma^2} e^{-\frac{x^2+y^2}{2\sigma^2}} \tag{4}$$

where x the distance from the origin in the horizontal axis, y is the distance from the origin in the vertical axis, and σ is the standard deviation of the Gaussian distribution and $g(x,y)$ is the smoothened image obtained using Gaussian smoothing filter. Subsequently, smoothened image $g(x,y)$ is manipulated in terms of its bit planes to extract the region of interest from enhanced wrist radiographs.

2.1 Region of interest extraction-bit plane slicing

Emphasizing analysis towards only the specific regions of interest in the problem domain increase the chances of reliability of the computerized diagnosis system. Performing manipulations at bit level further reduces the computational burden involved in processing of images. In this work, the region of interest extraction from smoothened image is performed using bit plane slicing. Number of bit planes in an image depends on the bit depth of pixels and categorized into high order and lower order bit planes. High frequency content is defined in higher order bit planes and low frequency content is

defined in lower order bit planes. The information in the bit planes is employed for extraction of wrist region in the images.

In this work, 8-bit images are subject to bit plane slicing and masks are generated by considering different combinations of higher order bit planes. If $b_1, b_2, b_3 \ldots b_k$ represents the bit planes sliced from a k-bit image then the masks M_1, M_2, M_3, M_4 are generated by reconstruction of different combinations of higher order bit planes. The core operations used for generation of masks M_1 to M_4 are carried out on basis of (5) and (8).

$$M_1 = \sum_i b_i \quad \text{for} \quad i = 5,6,7,8 \tag{5}$$

$$M_2 = \sum_i b_i \quad \text{for} \quad i = 2,3,7,8 \tag{6}$$

$$M_3 = \sum_i b_i \quad \text{for} \quad i = 5,6,7 \tag{7}$$

$$M_4 = \sum_i b_i \quad \text{for} \quad i = 6,7,8 \tag{8}$$

Masks M_1 to M_4 are employed as reference images for region of interest from gray scale counter parts of radiograph images. The optimal masks with in M_1 to M_4 leading to efficient performance of segmentation technique are analyzed subsequently in experimental analysis section.

2.2 Feature extraction and classification-convolutional neural networks (CNN)

Masks of wrist region generated from the preprocessed radiographs are used for accumulation of inputs to be fed to CNN, which automates feature extraction and classification of the wrist radiographs in two levels as indicated in the Fig. 1.

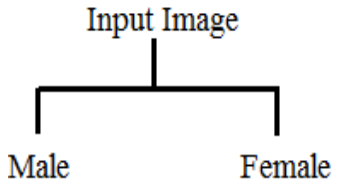

Figure 1: Classification model of wrist radiographs

2.3 Prediction of Gender-GeNet

GeNet is a pre trained model proposed in this work which is trained with masks generated from the pre-processed radiographs generated from bit plane based segmentation technique. The masks used to train the GeNet comprises of about 12559 images of both male (6833) and female (5726) including age groups ranging from 1 to 17 years. Fig. 2(a) and Fig. 2(b) depicts the instances of the masks adapted for training the GeNet for automatic feature extraction and recognition.

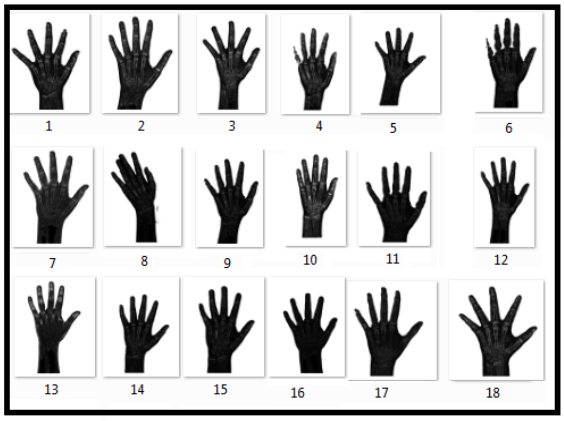

Figure 2(a): Instances of masks trained-Male

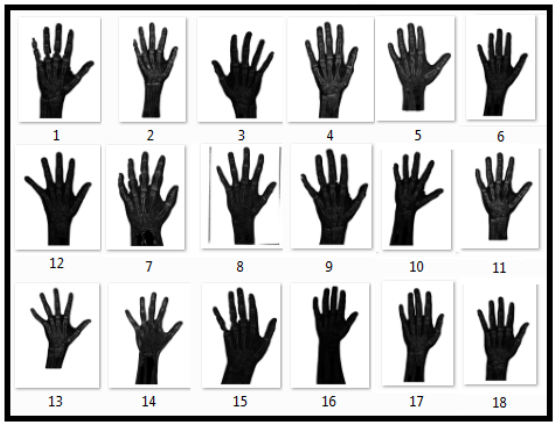

Figure 2(b): Instances of masks trained-Female

Masks of wrist region generated from the preprocessed radiographs are used for accumulation.

2.4 Architecture of GeNet

Convolutional neural network is a deep feed forward neural network where the conventional classifier models like support vector machine, regression network or any other fully connected networks are integrated with multiple levels of convolution process with max pooling as one of the core operation. A typical CNN architecture is built of input layer, multiple convolution layers with RELU+max pooling layer, hidden layers of feature vectors extracted through convolution process, fully connected layer where conventional classifiers are integrated and output layer as shown in Fig. 3. The performance of the CNN with numerous layers is better compared to other perceptron models of artificial neural networks which are intense in terms of number of computations due to presence of dense interconnections from layer to layer. Unlike perceptron models, CNN's can provide better performance due to feed forward design

and less number of layer to layer connections which leads to reduced computation of weights in the hidden layers.

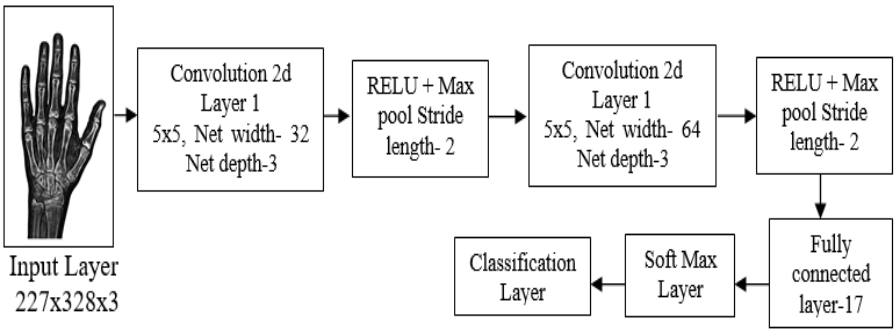

Figure 3: Architecture of GeNet

CNN's are widely used for image and data analysis tasks are a form of artificial neural networks defined of a set of hidden layers called convolution layers and non-hidden layers. Convolution layer accepts input from input layer and trains the input to the nodes in the current layer and forwards the output to the next layer. Precisely in the process of convolution, the patterns are detected and this requires the specification of number of filters using which convolution has to be carried along with the size of filters. Number of filters is usually designated as net width and the number of channels to be analyzed with respect to every pixel is net depth. Filters are instrumental in detection of variety of patterns including edges, corners, circles, texture and other geometrical structures that are inherent in the image. In GeNet, two hidden layers of convolution are integrated with 32 filters in level 1 and 64 filters in level 2 of convolution. More the deeper the network is, CNN's will be able to predict wider variety of patterns in the images leading to higher degrees of robustness of the deep learning system. Each filter plays a crucial role in detecting a particular type of pattern or objects as available in the image.

Convolution layer of GeNet is defined with 32 filters each of size 5×5 initially defined with some random numbers as indicated in the Fig. 4. Origin of the filter is overlaid with each pixel encompassing the neighborhood of 5×5 in the image. Each filter is convolved with 5×5 neighborhood of every pixel in the image until all the pixels exhausts. Convolution process provides the abstract representation of the image patterns in the form of the dot products, every 5×5 neighborhood of the image will be replaced by one pixel in the output of the image. Output of the convolution layer is the dot product representation of the input image.

0.35	0.7	0.2	0.74	0.89
0.78	0.14	0.25	0.3	0.92
0.8	0.28	0.75	0.25	0.17
0.97	0.45	0.6	0.56	0.22
0.22	0.41	0.7	0.23	0.55

Figure 4: Initialization of filter of 5×5

The feature visualization of dot product representation of input image after level 1 convolution is as depicted in Fig. 6. Each filter emphasizes specific gradient details in the input image comprising of complete gradient patterns. All these patterns detected are forwarded to max pooling layer for subsequent level of abstraction. Prior to the data being fed to max pool layer, the output of convolution layer will be fed to RELU (REctified Linear Unit) which is an integral part of max pool layer. RELU greatly improves the speed of training by adapting non linearity through $\tanh$ function being subject to differentiation. Let x be input to RELU, gradient computation is rectified to 0 or 1 depending upon the sign of x and response produced by RELU will be bound by (9).

$$0 \le \frac{\partial}{\partial x}\tanh(x) \le 1 \quad \forall x \in \left[-x_{\min}, +x_{\max}\right] \tag{9}$$

Response produced by RELU may lead to increase in nonlinearity in the output generated by convolution layer and overall effect of RELU on output image is resembled in terms of abruptly varying gray level discontinuities in the image. Subsequent to this, the response produced by RELU is fed to Max pool layer to perform down sampling of the data to provide higher level feature maps of an image leading to dimensionality reduction. In GeNet, max pool layer adapted a kernel of dimension 4×4 with stride length of "2" indicating the stepping down over the input in x and y direction without any overlap. Consider $m \times n$ is dimension of an image f with net depth of d then after down sampling using max pool function it will be reduced to $\frac{m}{2} \times \frac{n}{2} \times d$ as represented in the Fig. 5.

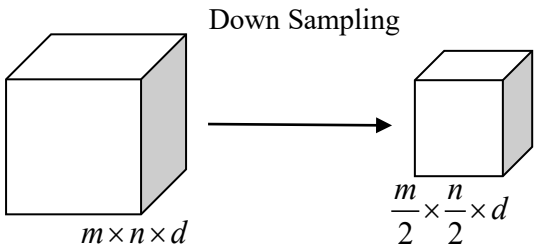

Figure 5: Protocol of max pool function

The higher level feature map obtained as result of max pool layer is further directed to undergo another level abstraction though hidden layer at convolution layer level 2, followed by RELU and max pooling functions. Finally fully connected layer employs a conventional classifier to classify the feature maps generated from the hidden layers. The probabilities of the predicted outcomes with respect to the number of classed are normalized with the help of soft max function prior to redirecting them to output layer. Genet is a pre trained model proposed in this work which is trained with masks generated.

3 Experimental analysis

In this work, performance of the algorithms implemented has been analyzed individually for bit plane slicing based segmentation and GeNet. Performance analysis of algorithms are conducted on datasets used in the Pediatric Bone Age Challenge contributed by Stanford University, the University of Colorado and the University of California-Los

Angeles available in Radiological Society of North America (RSNA), Radiology Informatics Committee (RIC) for pediatric bone age prediction. The bone age is represented in terms of number of months in the datasets considered and includes the children of age group starting from one year to 19 years of male and female.

The results of radiograph enhancement and outcome of bit plane slicing based segmentation technique along with the outcome of mask generation for combination of mask 1 and mask 2 clusters are as presented in the Fig. 6.

Performance of bit plane slicing segmentation technique is evaluated using the Jaccard similarity index $Jacc_{Ind}$, dice coefficient $Dice_{coe}$, false positive ratio fp_{rate} and false negative ratio fn_{rate}.

Tab. 1 represents the performance metrics of bit plane slice segmentation technique for few instances of masks extracted using combination of higher order bit planes 5, 6, 7 and 8 with its ground truths as depicted in Fig. 7.

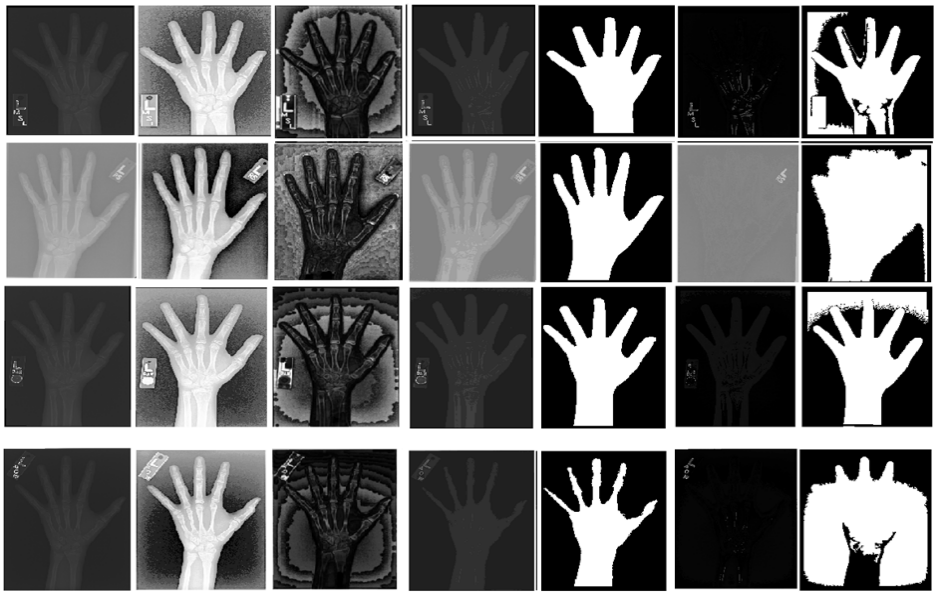

Figure 6: Outcome of radiograph enhancement and bit plane slicing segmentation technique (a) original image, (b) Equilized image, (c) Gaussian filtered-Smoothened image (d) Image with combination of higher order bit plane slices 5 to 8, (e) Mask generated by thresholding (d), (f) Image with combination of lower and higher order bit plane slices 2, 3, 7 and 8, (g) Mask generated by thresholding (f)

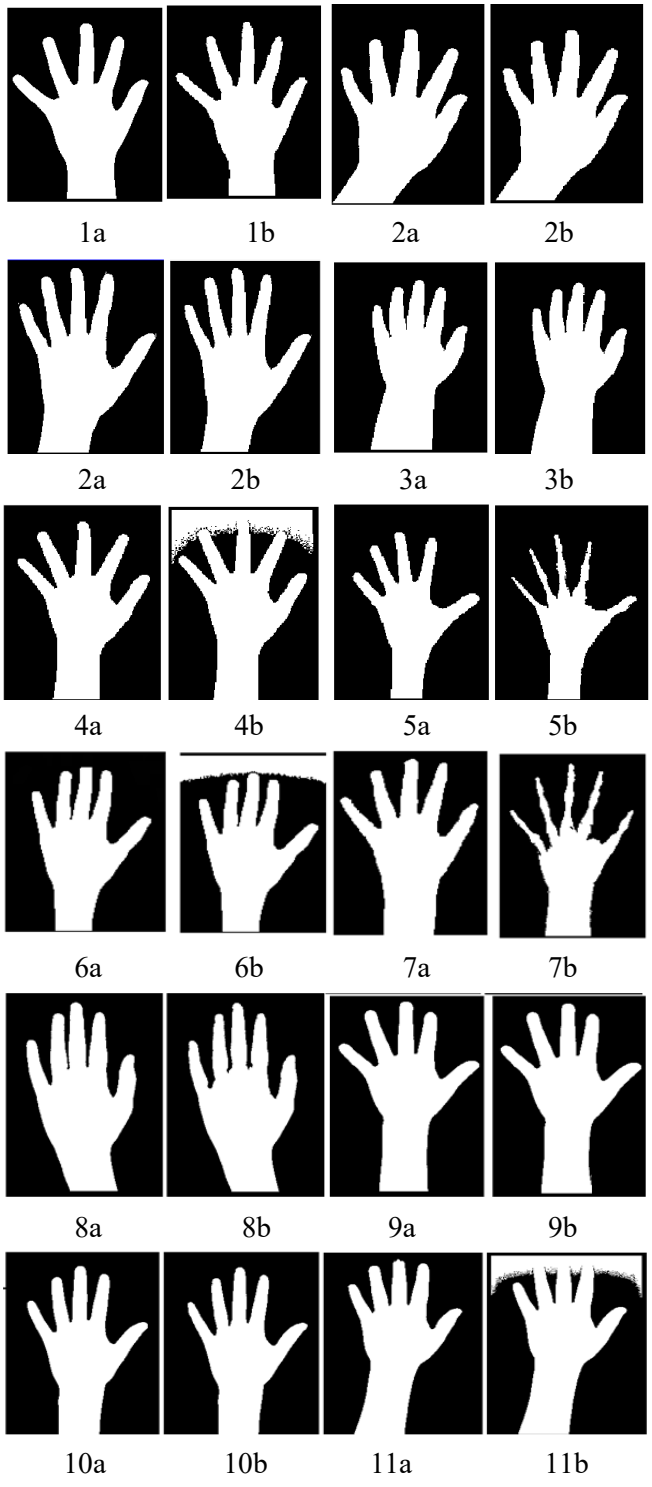
1a
1b
2a
2b
2a
2b
3a
3b
4a
4b
5a
5b
6a
6b
7a
7b
8a
8b
9a
9b
10a
10b
11a
11b

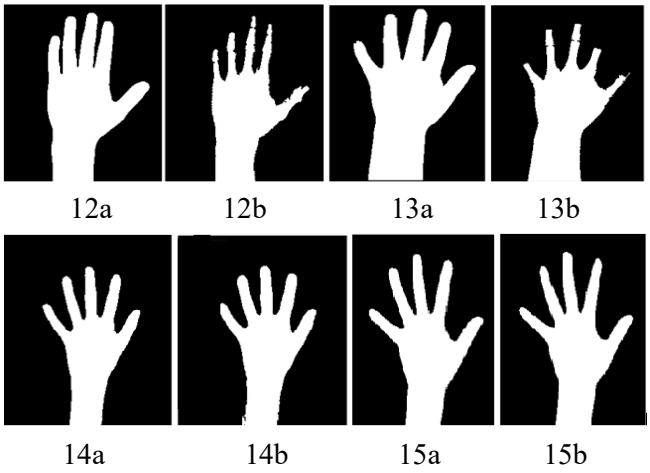

Figure 7: Few instances of ground truth and mask images generated using algorithm

Table 1: Performance of bit plane slice segmentation technique

Instance NO	$Jacc_{Ind}$	$Dice_{coe}$	fp_{rate}	fn_{rate}
1	0.9553	0.9772	0	0.0447
2	0.9904	0.9952	8.5168	0.0095
3	0.7303	0.8441	0	0.2697
4	0.9175	0.8374	0	0.0825
5	0.9494	0.9091	0	0
6	0.7716	0.8711	0	0.2284
7	0.9044	0.9498	1.7619	0.0954
8	0.5047	0.6708	0	0.4953
9	0.9361	0.9450	0.0903	0.0049
10	0.4954	0.6626	1.0184	0.0674
11	0.9666	0.9830	0	0.0334
12	0.6891	0.8159	0.3968	0.0375
13	0.7710	0.8707	0	0.2290
14	0.4436	0.6145	1.2545	0
15	0.4954	0.6626	1.0184	0.0674
16	0.9737	0.9867	0	0.0263
17	0.4772	0.6461	1.0955	0
18	0.4498	0.6205	1.2231	0.0150
19	0.8762	0.9340	0	0.1238

In the Fig. 8(a) and Fig. 8(b) counter parts of presented images indicates the ground truth and corresponding mask image generated using bit plane slicing segmentation algorithm. The ground truth masks are generated for over 1000 images and corresponding masks for the same are generated using segmentation algorithm for which the average Jaccard index is found to be 0.9255.

Figure 8(a): Female

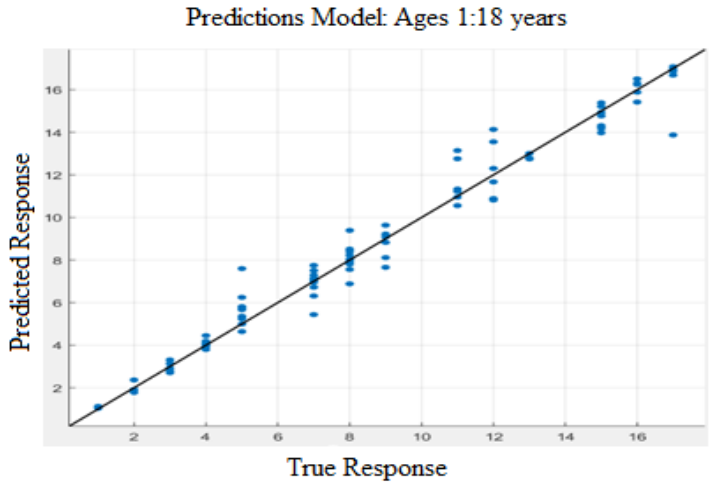

Figure 8(b): Male

Performance of GeNet is depicted in Fig. 9(a) and Fig. 9(b) indicating the prediction rate and loss of convergence between actual to mapped test instances for about 312 epochs.

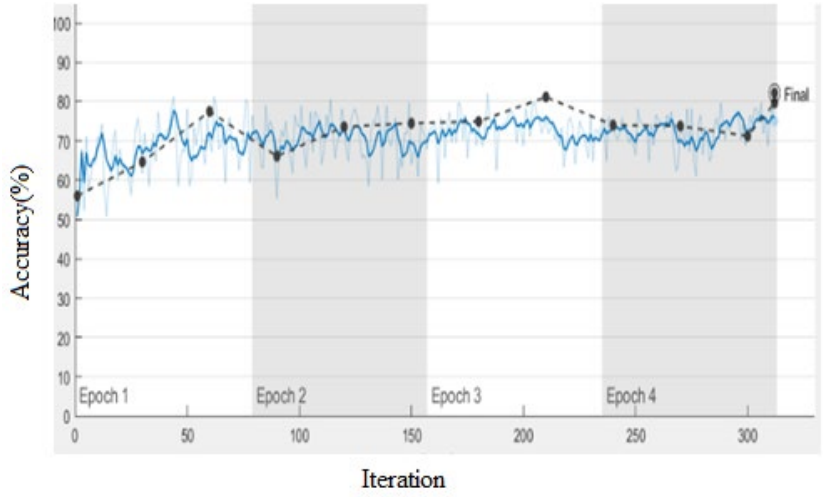

Figure 9(a): Performance of GeNet-Accuracy-Convolutional neural networks

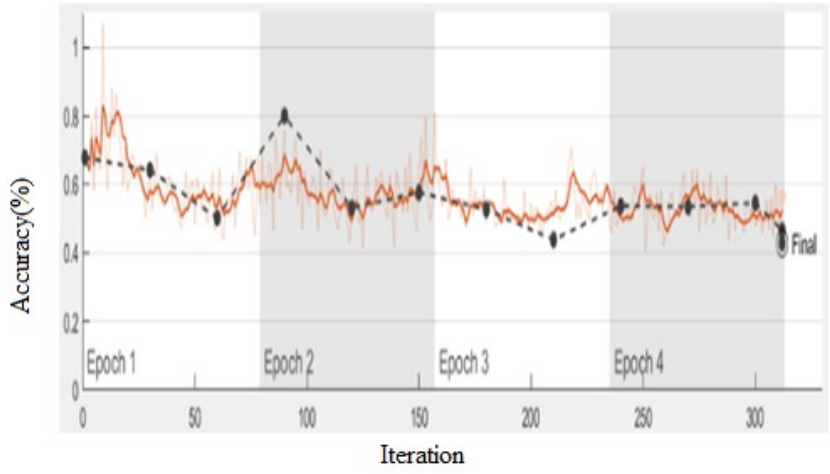

Figure 9(b): Performance of GeNet-Convolutional neural networks

4 Conclusions

In a nut shell, in this work gender assessment along with chronological age prediction of individual of age groups between one to 18 years is performed. Algorithmic technique contributions is done in terms of pre-processing, mask generation for wrist radiograph based on bit plane slices of radiograph image. A fully automated technique, GeNet architecture is devised for classification of radiographs based on the Gender using deep learning networks. Overall accuracy of the method developed seems to falls above 85% accuracy. The challenging part of the work lies in classification of the wrist radiographs into large number of classes when compared to other works in the same are focusing only 2

to 5 classes. Algorithms proposed are robust even with inconsistent illumination conditions of images indicating the uniqueness of proposed work.

Acknowledgement: Dataset Acknowledgements-we are very thankful to The Radiological Society of North America (RSNA) Radiology Informatics Committee (RIC) Pediatric Bone Age Machine Learning Challenge Organizing Committee and Stanford University, the University of Colorado and the University of California-Los Angeles.

Also, we are very thankful to Amrita Vishwa Vidyapeetham, Mysuru campus for providing the required technical support to execute deep learning algorithms. Also, we would like to acknowledge all the students of Department of Computer Science, Amrita School of Arts and Sciences contributed for creation of ground truth datasets for conducting experimentations.

Conflicts of Interest: The authors declare that they have no conflicts of interest to report regarding the present study.

References

Afifi, M.; Abdelhamed, A. (2019): AFIF4: deep gender classification based on adaboost-based fusion of isolated facial features and foggy faces. *Journal of Visual Communication and Image Representation*, vol. 62, pp. 77-86.

Aja-Fernández, S.; De Luis-Garcıa, R.; Martın-Fernandez, M. A.; Alberola-López, C. (2004): A computational TW3 classifier for skeletal maturity assessment-A computing with words approach. *Journal of Biomedical Informatics*, vol. 37, no. 2, pp. 99-107.

Bae, B. U.; Bae, W.; Jung, K. H. (2018): Improved deep learning model for bone age assessment using triplet ranking loss. *International Conference on Medical Imaging with Deep learning*, vol. 1, no. 1, pp. 1-3.

Bui, T. D.; Lee, J. J.; Shin, J. (2019): Incorporated region detection and classification using deep convolutional networks for bone age assessment. *Artificial Intelligence in Medicine*, vol. 97, pp. 1-8.

Bull, R. K.; Edwards, P. D.; Kemp, P. M.; Fry, S.; Hughes, I. A. (1999): Bone age assessment: a large scale comparison of the Greulich and Pyle, and Tanner and Whitehouse (TW2) methods. *Archives of Disease in Childhood*, vol. 81, no. 2, pp. 172-173.

Gertych, A.; Zhang, A.; Sayre, J.; Pospiech-Kurkowska, S.; Huang, H. K. (2007): Bone age assessment of children using a digital hand atlas. *Computerized Medical Imaging and Graphics*, vol. 31, no. 4, pp. 322-331.

Giordano, D.; Leonardi, R.; MaiorBaeana, F.; Scarciofalo, G.; Spampinato, C. (2007): Epiphysis and metaphysis extraction and classification by adaptive thresholding and DoG filtering for automated skeletal bone age analysis. *Annual International Conference of the IEEE Engineering in Medicine and Biology Society*, pp. 6551-6556.

Giordano, D.; Spampinato, C.; Scarciofalo, G.; Leonardi, R. (2010): An automatic system for skeletal bone age measurement by robust processing of carpal and epiphysial/metaphysial bones. *IEEE Transactions on Instrumentation and Measurement*,

vol. 59, no. 10, pp. 2539-2553.

Hsieh, C. W.; Liu, T. C.; Jong, T. L.; Tiu, C. M. (2010): A fuzzy-based growth model with principle component analysis selection for carpal bone-age assessment. *Medical & Biological Engineering & Computing*, vol. 48, no. 6, pp. 579-588.

Kontos, D.; Megalooikonomou, V.; Gee, J. C. (2009): Morphometric analysis of brain images with reduced number of statistical tests: a study on the gender-related differentiation of the corpus callosum. *Artificial Intelligence in Medicine*, vol. 47, no. 1, pp. 75-86.

Lee, H.; Tajmir, S.; Lee, J.; Zissen, M.; Yeshiwas, B. A. et al. (2017): Fully automated deep learning system for bone age assessment. *Journal of Digital Imaging*, vol. 30, no. 4, pp. 427-441.

Mahmoodi, S.; Sharif, B. S.; Chester, E. G.; Owen, J. P.; Lee, R. (2000): Skeletal growth estimation using radiographic image processing and analysis. *IEEE Transactions on Information Technology in Biomedicine*, vol. 4, no. 4, pp. 292-297.

Mansourvar, M.; Ismail, M. A.; Herawan, T.; Gopal Raj, R.; Abdul Kareem, S. et al. (2013): Automated bone age assessment: motivation, taxonomies, and challenges. *Computational and Mathematical Methods in Medicine*, vol. 2013, pp. 1-11.

Martin, D. D.; Deusch, D.; Schweizer, R.; Binder, G.; Thodberg, H. H. et al. (2008): Clinical application of automated Greulich-Pyle bone age determination in children with short stature. *Pediatric Radiology*, vol. 39, pp. 598-607.

Michael, D. J.; Nelson, A. C. (1989): HANDX: a model-based system for automatic segmentation of bones from digital hand radiographs. *IEEE Transactions on Medical Imaging*, vol. 8, no. 1, pp. 64-69.

Mwaturura, T.; Cloutier, F. C.; Daneshvar, P. (2019): Analysis of radiographic relationship between distal radius, Ulna, and Lunate. *Journal of Wrist Surgery*.

Pietka, E.; Gertych, A.; Pospiech, S.; Cao, F.; Huang, H. K. et al. (2001): Computer assisted bone age assessment: image preprocessing and epiphy-seal/metaphyseal ROI extraction. *IEEE Transactions on Medical Imaging*, vol. 20, no. 8, pp. 715-729.

Pietka, E.; Gertych, A.; Pospiech, S.; Cao, F.; Huang, H. K. et al. (2001): Computer-assisted bone age assessment: image preprocessing and epiphyseal/metaphyseal ROI extraction. *IEEE Transactions on Medical Imaging*, vol. 20, no. 8, pp. 715-729.

Pietka, E.; Kaabi, L.; Kuo, M. L.; Huang, H. K. (1993): Feature extraction in carpal bone analysis. *IEEE Transactions on Medical Imaging*, vol. 12, no. 1, pp. 44-49.

Rai, P.; Khanna, P. (2014): A gender classification system robust to occlusion using Gabor features based (2D) 2PCA. *Journal of Visual Communication and Image Representation*, vol. 25, no. 5, pp. 1118-1129.

Santosh, K. C. (2019): Development of human age and gender identification system from teeth, wrist and femur images. *International Conference on Sustainable Computing in Science*, *Technology and Management*.

Simu, S.; Lal, S. (2017): Automated bone age assessment using bag of features and random forests. *International Conference on Intelligent Sustainable Systems*, pp. 911-915.

Tanner, J. M.; Gibbons, R. D. (1994): Automatic bone age measurement using

computerized image analysis. *Journal of Pediatric Endocrinology and Metabolism*, vol. 7, no. 2, pp. 141-146.

Thangam, P.; Mahendiran, T. V.; Thanushkodi, K. (2012): Skeletal bone age assessment-research directions. *Journal of Engineering Science & Technology Review*, vol. 5, no. 1, pp. 1-6.

Tristán-Vega, A.; Arribas, J. I. (2008): A radius and ulna TW3 bone age assessment system. *IEEE Transactions on Biomedical Engineering*, vol. 55, no. 5, pp. 1463-1476.

Villar, P.; Alemán, I.; Castillo, L.; Damas, S.; Cordón, O. (2017): A first approach to a fuzzy classification system for age estimation based on the pubic bone. *International Conference on Fuzzy Systems*, pp. 1-6.

Wang, S.; Shen, Y.; Shi, C.; Yin, P.; Wang, Z. et al. (2018): Skeletal maturity recognition using a fully automated system with convolutional neural networks. *IEEE Access*, vol. 6, pp. 29979-29993.